Progress In Electromagnetics Research B, Vol. 86, 139–158, 2020

H-Shaped Fractal Slots Based Highly Miniaturized Substrate Integrated Waveguide Metamaterial Bandpass Filters for C-Band Applications

Ayad M. Hamzah[1, 2, *], Lukman Audah[1], and Nasr Alkhafaji[3]

Abstract—A new family of substrate integrated waveguide SIW-metamaterial bandpass filters is proposed which support backward and forward wave propagations with two adjacent passbands under the cutoff frequency of the conventional SIW structure. Through varying the fractal slots sizes etched over SIW structures, different frequency transmission responses were realized. Extraction of the metamaterial parameters was achieved via scattering parameters. The equivalent electrical length of a fractal slot is larger than the conventional slot, making it suitable to design highly miniaturized filters. The equivalent circuit model was analyzed in detail to provide comprehension on the SIW-metamaterial unit cells. Three filters using the 3rd iteration H-shaped SIW-metamaterial unit cells were designed and tested using subwavelength resonators. Filter design was used to extract the coupling coefficient and external quality factor to obtain the filters' optimized physical dimensions. The out-of-band rejection can be enhanced by reconfiguring the fractal slots or the SIW. A wide upper out-of-band rejection with attenuation > 30 dB with the range 5.5 GHz to 8 GHz was realized. The proposed filters offer advantages through low insertion loss, easy fabrication, high selectivity, small size, and low cost. The measured scattering parameters S_{21} and S_{11} were in good agreement with the simulated ones.

1. INTRODUCTION

Bandpass filters (BPFs) are one of the main components of transceivers as in image-reject or band-select types. Filters with low insertion loss and high rejection to interferences fallen out of the interesting band, relaxing requirements of large dynamic ranges of different components, such as mixers and low noise amplifiers (LNAs) in the existence of crowded Radio frequency RF environments, are preferred. Filters designed based on waveguides have high quality factors and low losses, but they are bulky devices. Thus, the alternative possible option to exploit the significant properties of waveguides to design good filters is the printed or substrate integrated waveguide (SIW) [1–3]. However, the main drawback of these filters is their big size because they work above the cutoff frequency [4, 5]. Dong et al. proposed a new technique which is called metamaterial, allowing microwave filters to work below cutoff frequencies of waveguides [5].

Theoretical concepts of the metamaterial were presented for the first time by Veselago five decades ago [6]. About two decades ago, Smith et al. implemented the first practical experiment using metamaterial structures. The difference between the material found in nature and the metamaterial that does not exist in nature is that the metamaterial has simultaneously negative permeability and permittivity. These unusual properties enable researches to design a new family of microwave and millimeter wave components [7, 8]. Double negative (DNG) material and left-handed material (LHM)

Received 30 December 2019, Accepted 8 February 2020, Scheduled 4 March 2020

* Corresponding author: Ayad Muslim Hamzah (Engayad79@atu.edu.iq).

[1] Faculty of Electrical and Electronic Engineering, University Tun Hussein Onn Malaysia, Parit Raja 86400, Malaysia. [2] Technical Institute of Najaf, Al-Furat Al-Awsat Technical University, Iraq. [3] Engineering Technical College of Al Najaf, Al-Furat Al-Awsat Technical University, Iraq.

are other names for the metamaterial found in the literature. The split ring resonators (SRRs) and thin wires are the main components utilized by Shelby et al. to realize the well-known DNG metamaterials [9]. The thin wires provide negative permittivity, while the SRRs provide negative permeability. Based on the duality concepts, Falcone et al. proposed complementary split ring resonators (CSRRs) which provide negative permittivity if they are axially excited by an electrical field [10, 11]. In addition to that, the slot can provide negative permeability [12]. Thus, these four elements (SRRs, thin wires, CSRRs, and slots) are the key components, and they attract big interest among researchers to build metamaterials microwave components having small size and high selectivity. SRRs and slots behave as magnetic dipoles, whereas CSRRs and thin wires act as electrical dipoles. All these four elements can be realized using the planar technology such as microstrip and coplanar waveguide (CPW).

SIW is a planar counterpart of the conventional rectangular waveguide introduced for the first time about two decades ago [1]. The dispersion and propagation characteristics of SIW are similar to what the rectangular waveguide has. SIW consists of two rows of vias drilled along the longitudinal edges of a substrate and connected by two metal plates connected at the bottom and top faces of the substrate. SIW structures attract researchers to design a variety of microwave components with high quality Q-factor, low cost, and high-power handling. As mentioned above, the only problem that SIW structures suffer is large size [13]. There are several ways to miniaturize such devices designed using SIW structures, especially in low frequencies. A folded SIW is one of the ways where the width of the original SIW structure is cut to half [14]. Also, the original width of the SIW can be reduced by 40% by adding a central row of vias, called ridge SIW [15]. Exploiting fictitious magnetic walls to obtain a reduced SIW, namely half-mode SIW (HMSIW) and quarter-mode SIW (QMSIW), has been proposed, studied, and analyzed with the same behavior as that of the conventional rectangular waveguide bandpass filters [16–18]. All ratios of miniaturization attained by these techniques cannot exceed 50% compared to the classical SIW prototypes.

Surprisingly, SIW structures automatically provide effective negative permittivity when working under the cutoff frequency of the dominant mode TE_{10} without utilizing any type of resonant structure. Waves with frequencies smaller than the cutoff frequency cannot propagate, called evanescent waves. This property seems impractical in conventional waveguide components, but it turns out very interesting under the scenario of DNG metamaterials [19]. By allowing the evanescent waves to propagate inside SIW structures and to make them work under the cutoff frequency, miniaturization ratios higher than 50% can be attained easily. This is called the evanescent-mode technique. There are two options to convert the evanescent into propagating modes. The first option is to convert the negative permittivity to the positive called the forward propagation (i.e., both permittivity and permeability positive), and the second option is to make the permeability negative called the backward propagation (i.e., both permittivity and permeability negative). Based on the evanescent-mode technique, when either the electric or magnetic dipoles are loaded on the top wall of the SIW, forward or backward passbands below the cutoff frequency of the SIW can be obtained. Different filter designs using the electric dipoles (i.e., CSRRs) etched on the top wall of the SIWs are proposed in the order of the miniaturization [5, 20, 21]. Also, the fractal and stepped impedance resonator (SIR)-CSRRs are proposed to get further miniaturization [22, 23]. When using the SIR-CSRR, each arm in the CSRRs is replaced by its equivalent slotted SIR arrangements. The aim of using SIR configurations is to highly reduce the SIW-metamaterial unit cells. Backward wave propagation which is another option is realized by loading the magnetic dipoles (i.e., slots) over the top walls of the SIW structures. Most designs that use this method are antennas [24], but in our designs, we will use this method to realize compact and high-performance filters. In [24], interdigital slots working as capacitors are used instead of classical slots as a step to efficiently occupy all the top surfaces of the SIW structures.

In this research paper, fractal slots are used as magnetic dipoles because of their capability to fill spaces of the top surfaces of SIW structures. Very compact SIW-metamaterial unit cells and filters are expected as a result of using very long slots. Based on the principles of the complementarity and duality, fractal slots can be derived from conventional fractal transmission lines. SIW-metamaterial unit cells with different iterations which are the 1st, 2nd, and 3rd will be presented and investigated. Filters using the 3rd iteration fractal slots will be designed, simulated, fabricated, and tested. The proposed miniaturized SIW-metamaterial unit cells with fractal slots could provide negative permeability and permittivity at the same time at a specific frequency band. However, our proposed designs also convert

the negative permittivity to the positive at another frequency band. Fortunately, these two bands are very close to each other, adjacent bands, with no gap. According to the best of the authors' knowledge, SIW-metamaterial unit cells and filters supporting both backward and forward wave propagations will be introduced for the first time as an original contribution.

Finally, this paper is organized as follows. In Section 2, H-shaped fractal slots based SIW-metamaterial unit cells are investigated in detail. This section includes different parts to cover all the required information useful for understanding our work. Section 3 explains the Filter Design Methodology. Next, in Section 4, the simulation and measurement results are presented. Section 5 introduces the conclusion.

2. FRACTAL METAMATERIAL-SIW UNIT CELLS

Configurations of fractal curves are first introduced in this section, followed by the working principles of the proposed SIW-metamaterial unit cells. Extraction of the effective SIW-metamaterial parameters of unit cells are then presented to demonstrate that the proposed unit cells can work under the cutoff frequency of the SIW with the scenarios of backward propagation (i.e., double negative DNG metamaterial) and forward propagation (i.e., double positive DPS metamaterial). At the end of this section, the equivalent circuit model is derived and analyzed, and losses caused by the different factors are demonstrated.

2.1. Fractal Curves

The end of the 19th century witnessed the emergence of fractal geometry when Peano proposed a continuous curve passing through all points of a specified space [25]. A successive repetition of one specific geometrical form, in an iterative manner, was used to generate fractal curves. In other words, it can be described as a collection of scaled replicas of the first form. The higher orders of fractal curves obtained after each iteration have longer curves than those generated in the preceding iterations to entirely fill the given area where they were generated. The space-filling property of the fractal geometry was exploited to highly miniaturize passive microwave components because, theoretically, traces (lines) with infinite-lengths can be realized on small areas.

Some designs using a fractal geometry have shown that very compact antennas, resonators, and filters can be realized due to its very long microstrip lines being printed on small given substrates. Also, a wide variety of applications such as high impedances surfaces HISs [26], frequency selective surfaces FSSs [27], RF identifications [28], and left-handed metamaterials LHMs [29] utilized the fractal geometry to design multi-band and small structures.

The non-integer dimension is a property of fractal curves which is between 1 and 2 for planar fractal curves. It can be considered as a measure of how the fractal curves can fill small regions. The ratio in Eq. (1) can be used to calculate the dimensions of the fractal curves,

$$D = \frac{\log(k)}{\log(r)} \tag{1}$$

where k is the number of self-similar segments of the fractal curves attained from one segment after each iteration, and r is the number of segments obtained from one segment in each iteration. Figure 1

Figure 1. A comparison between the conventional straight-line (e.g., transmission-line) and its length-equivalent fractal curve.

displays a conventional transmission-line (i.e., straight line with a specific width) and its equivalent fractal configuration. Ideally, although the fractal transmission-line can be printed on a small area, both fractal curves and the conventional transmission-line may have the same electrical length. Using fractal geometry allows the use of shorter transmission-lines, but with longer equivalent electrical length. This aids to miniaturize transmission-lines, being a key part to the miniaturization processes of microwave circuits and antennas.

Today, there are a lot of fractal curves which are well known such as Piano, Koch, and Serpiniski. In order to determine which fractal curve is suitable for our design, some criteria should be considered in advance. The miniaturization ratio that a fractal curve can introduce is one of the intentions considered in this research study, so dimensions of the fractal curve are chosen as the most important parameter. The fractal curves which reach dimension 2 are better because of its ability to efficiently fill in small areas, therefore obtaining very compact devices. Several fractal curves have dimensions equal to 2 which is the maximum value, and Figure 2 shows some of them such as H-shaped, Piano, and Hilbert fractal curves. In our design, H-shaped fractal curve is chosen over others for reasons shown later in this research work. Figure 3 depicts the process of the H-shaped fractal curve generation. As can be seen,

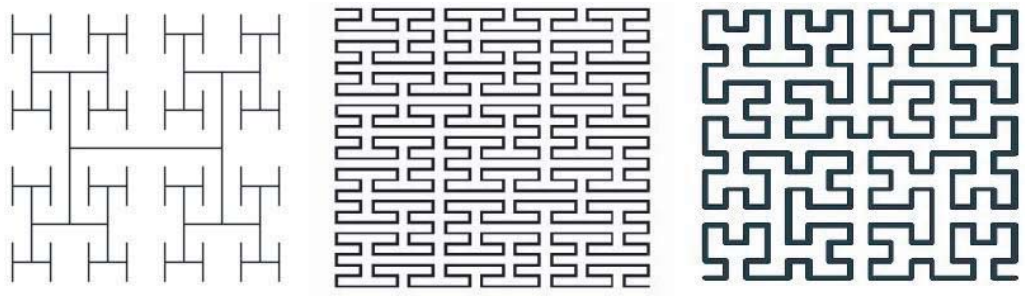

Figure 2. Three types of fractal curves (H-shaped, Piano, and Hilbert).

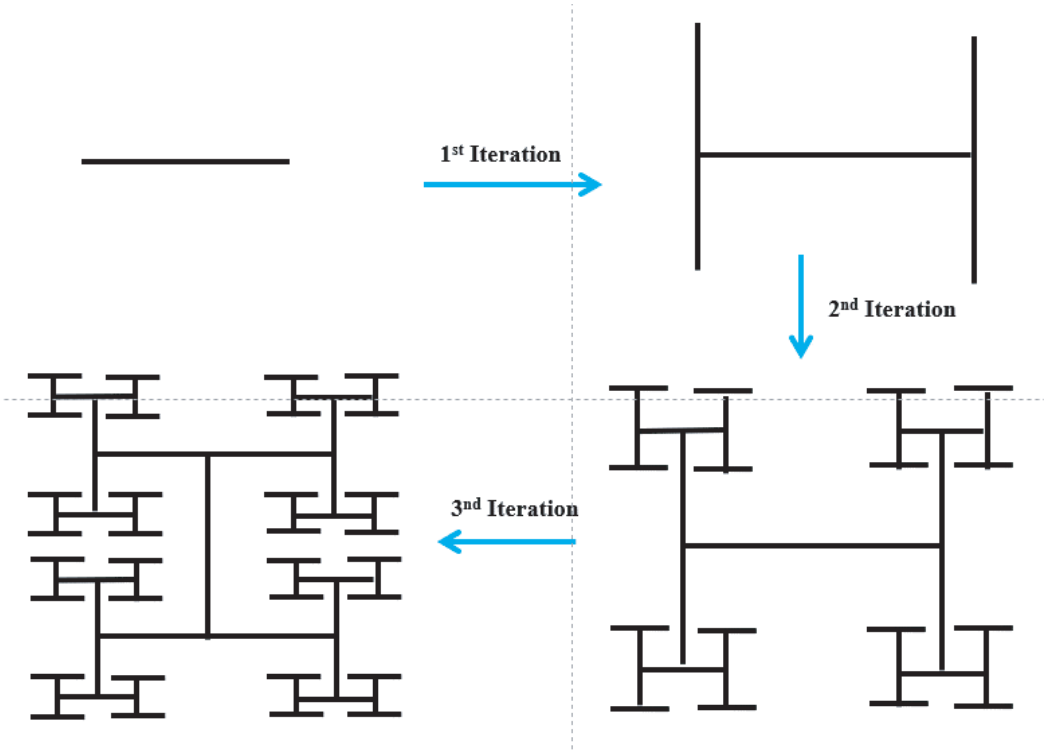

Figure 3. Process of the H-shaped fractal curve generation.

the dimension of an H-shaped fractal curve tends to reach 2 with the increase of an iteration order, filling the whole given area.

2.2. Working Principles of the Proposed SIW-Metamaterial Unit Cells

In the proposed work, the conventional H-shaped fractal transmission-lines are replaced with their counterparts which are H-shaped fractal slots. According to a fractal iteration, the 3rd iteration was chosen to fulfill the design requirements. Typically, a conventional slot etched below a microstrip transmission-line, shown in Figure 4(a), is utilized to realize the negative permeability in the vicinity of the resonant frequency. Thus, the proposed H-shaped fractal slot is also used to obtain the effective negative permeability. Extraction of the real parts of permittivity ε and permeability μ (i.e., constitutive parameters) of the 3rd iteration H-shaped fractal slot etched beneath a transmission-line on the ground using the S-parameters is depicted in Figure 4(b), and Figure 4(c) displays the comparison between the effective permeability μ of the conventional and fractal slots. The figure shows that the negative permeability is from about 6 GHz to 7.9 GHz, with a bandwidth about 1.9 GHz for the structure with the fractal slot, whereas the negative permeability is from about 5.4 GHz to 8 Hz, with a bandwidth about 2.6 GHz for the structure with the conventional slot. Moreover, the permittivity is still positive for both structures and for all frequencies. Hence, evanescent waves occur, resulting in band-stop filters BSFs at these two frequency bands.

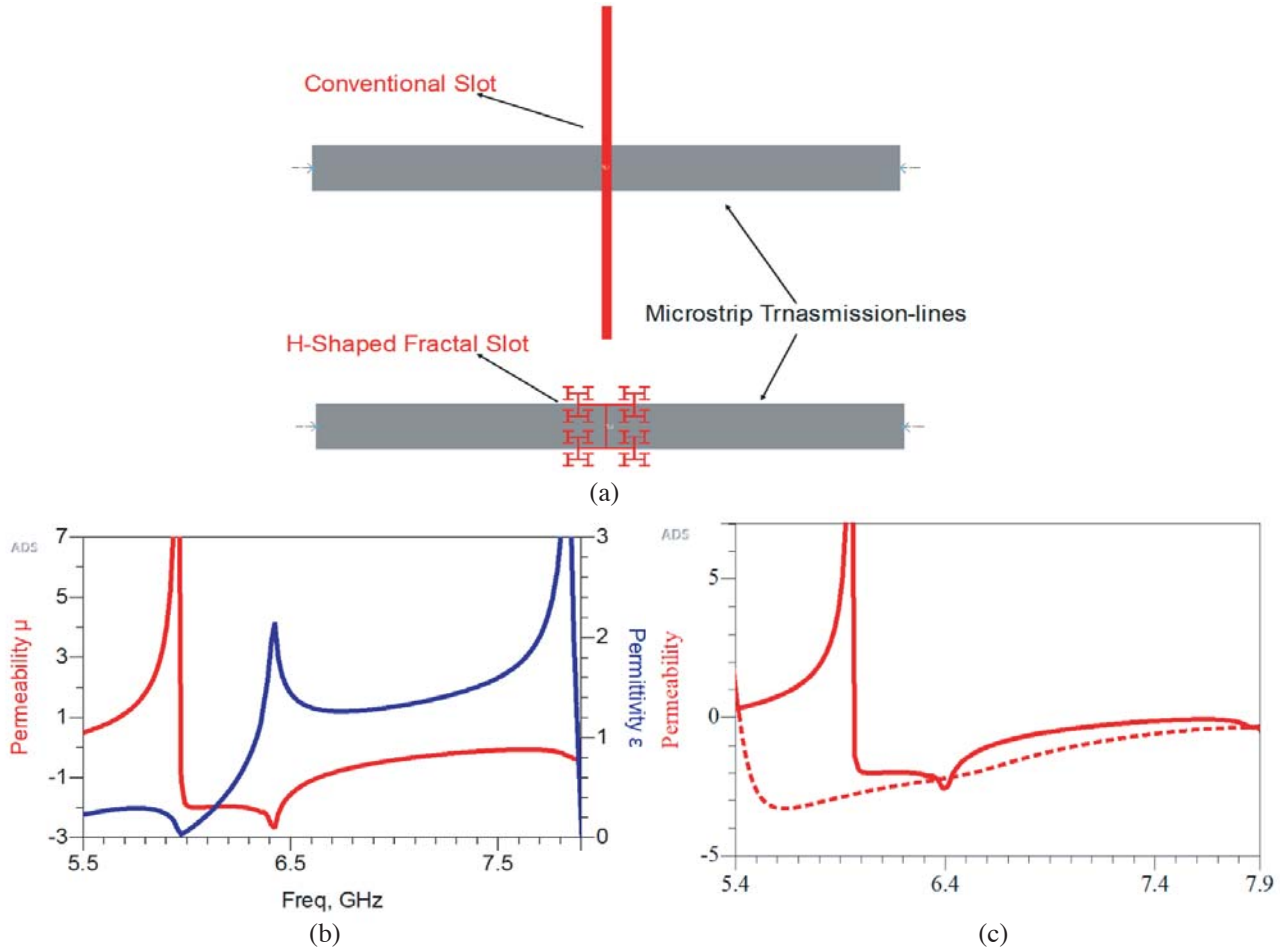

Figure 4. (a) Structures with conventional and H-shaped fractal slots, (b) the effective permeability and permittivity of a structure with the 3rd H-shaped fractal slot, (c) a comparison between the effective permeability of a structure with the 3rd H-shaped fractal slot (solid-line) and a structure with the conventional slot (dashed-line).

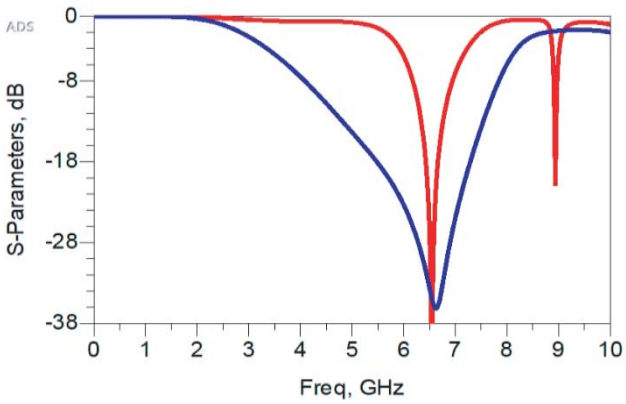

Figure 5. Simulated frequency responses (S_{21} — insertion-losses or transmission coefficients) of a structure with the 3rd H-shaped fractal slot (red-line) and a structure with the conventional slot (blue-line).

Figure 5 depicts the comparison between the S-parameters of the conventional and the 3rd iteration H-shaped fractal slots, etched on the ground of the conventional microstrip transmission-lines. As can be seen, both structures impede signals to pass from one port to another around the same frequency although the two responses do not have the same bandwidth. The miniaturization due to the space filling property of the fractal geometry can be observed. From the response of the fractal slot, there is another band around the frequency of 8.85 GHz, confirming the multiband property that fractal structures have. Consequently, if the H-shaped fractal slot has the same side length as the length of the conventional slot, a frequency of the fractal slot will decrease to lower frequencies.

In order to obtain metamaterial structures, parameters ε and μ should be negative. This is as in the proposed filter which uses the substrate integrated waveguide SIW as a transmission-line instead of the conventional microstrip transmission-line. The SIW provides negative permittivity under the cutoff frequency. This results in the proposed design to be simpler than other metamaterial structures (i.e., unit-cells) [19]. As shown above, the slot which acts as a magnetic dipole provides negative permeability at specific bands of frequencies. The fractal slots are etched over the broad (top) walls of the SIW structures. However, slots can also be etched on the grounds of the SIW structures, introducing the same responses. However, keeping the ground solid, it is preferred to reduce the noise and radiation losses in high-frequency radio systems.

In order to achieve high coupling between the SIW structures and fractal slots, the fractal slots are etched at centers of the waveguides, exciting by the maximum electric field of the fundamental mode TE_{10}. Figure 6 shows three metamaterial unit cells along with the conventional SIW structure. The

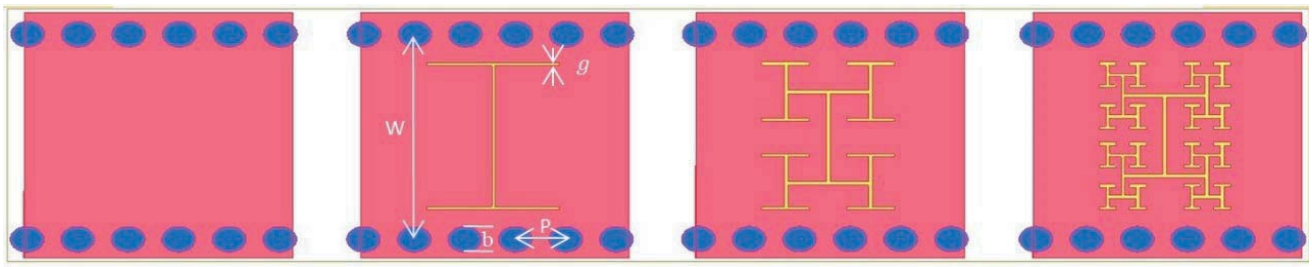

Figure 6. (a) Conventional SIW, (b) the 1st iteration H-shaped fractal SIW-metamaterial unit cell, (c) the 2nd iteration H-shaped fractal SIW-metamaterial unit cell, (d) the 3rd iteration H-shaped fractal SIW-metamaterial unit cell.

SIW structures-based metamaterial unit cells with the 1st, 2nd, and 3rd iterations of H-shaped fractal slots are introduced. An FR4 substrate with thickness $h = 1.2$ mm and dielectric constant $\varepsilon_r = 4.6$ was used in all simulations and fabrications. The width of the SIW w_{eff} was 7.8 mm to have the cutoff frequency at about 10.3 GHz; the via diameter a was 1 mm, the distance between any two successive vias b was equal to 1.5 mm; the side length of the fractal curve p was 6.4 mm; and the slot width g was 0.15 mm. Figure 7 displays the S-parameters of the conventional SIW and the SIW based fractal metamaterial unit-cells. As can be seen, metamaterial unit cells allow signals to pass through them under the cutoff frequency of the SIW structures which was about 10.3 GHz, while the conventional SIW prohibits signals under that cutoff frequency, having evanescent modes. Thus, we can name them as evanescent resonators. Figure 8 displays the current distributions of the conventional SIW structure and the 3rd iteration H-shaped fractal SIW-metamaterial unit cell to confirm that signals can propagate inside the proposed fractal SIW-metamaterial unit cells while being prohibited from propagation inside the conventional SIW structure under the cutoff frequency, for example, at 5 GHz. In addition to that, the current distributions of the 3rd iteration H-shaped fractal SIW-metamaterial unit cell at 3 GHz and 8 GHz have been illustrated to show that the structure can also prohibit signals from propagation outside

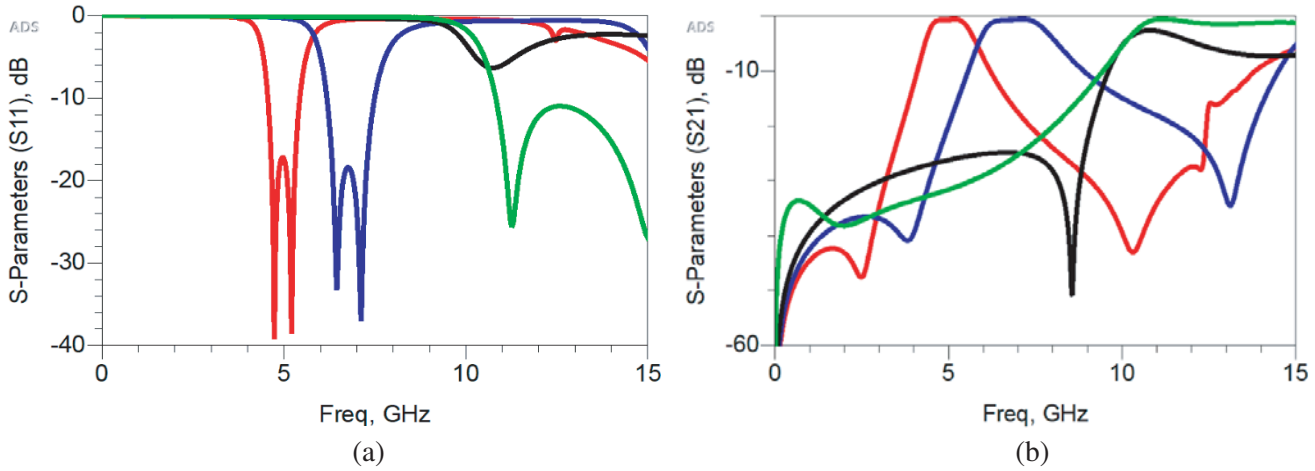

Figure 7. (a) Frequency responses (S_{11}) of structures shown in Figure 6(a) (green line), Figure 6(b) (black line), Figure 6(c) (blue line), and Figure 6(d) (red line), (b) frequency responses (S_{21}) of structures shown in Figure 6(a) (green line), Figure 6(b) (black line), Figure 6(c) (blue line), and Figure 6(d) (red line).

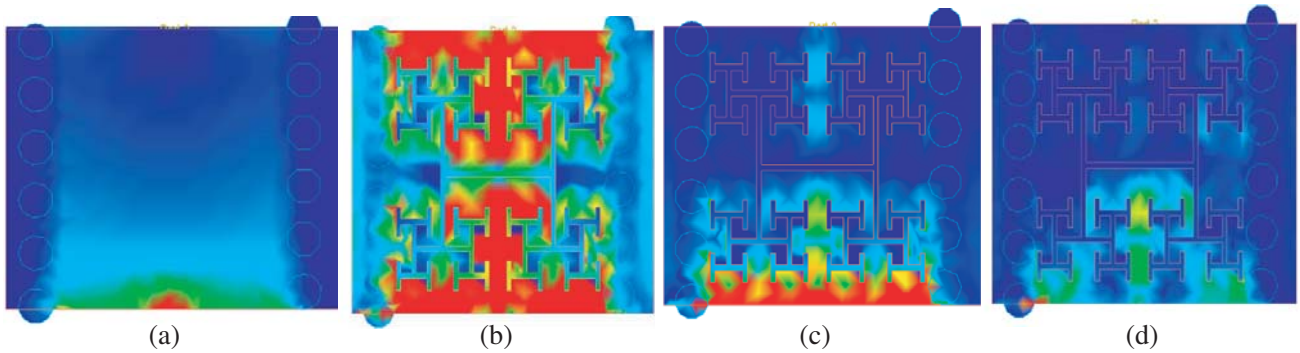

Figure 8. (a) Current distribution inside the conventional SIW at a frequency of 5 GHz, (b) current distribution inside the 3rd iteration H-shaped fractal SIW-metamaterial unit cell at a frequency of 5 GHz, (c) current distribution inside the 3rd iteration H-shaped fractal SIW-metamaterial unit cell at a frequency of 3 GHz, (d) current distribution inside the 3rd iteration H-shaped fractal SIW-metamaterial unit cell at a frequency of 10 GHz.

the allowed band. These figures give a quick glance to see which frequency can be distributed inside the proposed unit cells. The normal components of the dominant electrical fields extending from the ground to the broad wall of the SIW structure excite the fractal slots acting as magnetic dipoles, while components of the magnetic field are parallel to the top wall of the SIW and are normal to the sidewalls. Moreover, the center frequency of the passband decreases as the fractal iteration increases. Although the frequency response of the 1st iteration H-shaped fractal SIW-metamaterial unit cell has a passband slightly below the cutoff frequency of the conventional SIW structure, the emergence of the passband, at the frequency 10.1 GHz, was clear. In other words, the typical responses of waveguides which were highpass were turned into bandpass. Center frequencies of the 2nd and 3rd iterations H-shaped fractal SIW-metamaterial unit cells were 6.875 GHz and 4.959 GHz, respectively. Maintaining the same side lengths for different iterations of the fractal slots inside the SIW-metamaterial unit cells having the same overall size resulting in responses with different frequencies, which was equivalent to reduction in size. The reduction ratios of the 2nd and 3rd iterations H-shaped fractal SIW-metamaterial unit cells compared to the 1st iteration unit cell were equal to 32.9% and 51.6%, respectively. The 2nd and 3rd iterations H-shaped fractal SIW-metamaterial unit cells offer good filtering responses as illustrated in Figure 7. The fractal slots etched on SIW structures introduced two transmission poles where two non-identical modes were excited and coupled. Furthermore, two transmission zeros were introduced as well, leading to enhancing the filtering selectivity. The fractal SIW-metamaterial unit cells had highpass characteristics located after the passbands which moved to higher frequencies than the cutoff frequency of the initial SIW structures. This phenomenon occurs because the proposed fractal SIW-metamaterial unit cells squeeze the primary TE_{10} modes by slots, resulting in shorter guides. For more details, readers can refer to [5].

2.3. Extraction of Metamaterial Parameters

To better clarify the principles of the backward transmission of passbands under the cutoff frequency of the SIW structure, the proposed metamaterial unit cells were analyzed and investigated to demonstrate that they have negative permittivity and permeability at specific bands. Only the SIW-metamaterial unit cell with the 3rd iteration H-shaped fractal slot was chosen to extract its effective metamaterial parameters for the sake of simplicity. The transmission response of the 3rd iteration H-shaped fractal SIW-metamaterial unit cell was centered almost at 5 GHz, compared to the response of the conventional SIW with the same overall dimension as shown in Figure 9(a). The overall size of the fractal slot plays a vital role in determining the center frequency for the passband, so three different sizes for the 3rd iteration H-shaped fractal slots were engraved on the top wall of the SIW structure. These sizes were

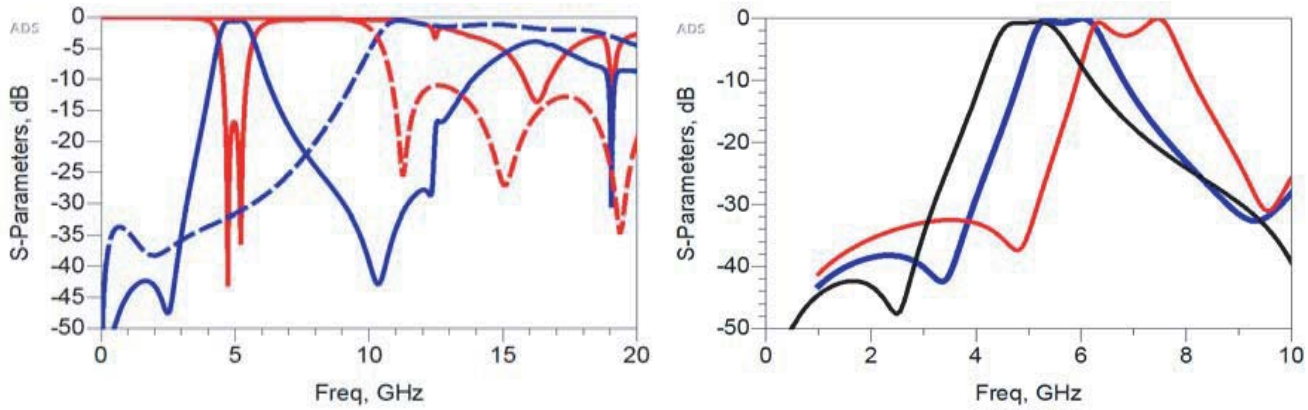

Figure 9. (a) A comparison between the frequency (scattering) response of the 3rd iteration H-shaped fractal SIW-metamaterial unit cell (solid line) and the conventional SIW (dashed line) S_{21} is blue and S_{11} is red, (b) the transmission coefficient (S_{21}) of the 3rd iteration H-shaped fractal SIW-metamaterial unit cell for three different fractal slot sizes of $p = 4.5$ mm is red, 5.5 mm is blue, and 6.5 mm is black.

with a side length of $p = 4.5\,\text{mm}$, $5.5\,\text{mm}$, and $6.5\,\text{mm}$. As the overall size of a fractal slot increases, the frequency decreases as shown in Figure 9(b) where the insertion losses S_{21} are presented. The bigger size of the 3rd iteration H-shaped fractal slot was adopted in all our future designs. Figure 10(a) shows the simulated permittivity and permeability of the 3rd iteration H-shaped fractal-SIW-metamaterial unit cell. As illustrated in the figure, the shaded areas are where both the permittivity and permeability were simultaneously negative or positive, supporting the backward or forward propagation. These two effective metamaterial parameters were extracted depending on the simulated S-parameters. From the results, we can deduce that there are two different types of propagations relying on the signs of permittivity and permeability. They are negative at a frequency range of about $4.4\,\text{GHz}$ to $5.15\,\text{GHz}$, while they change their signs into positive from about $5.15\,\text{GHz}$ to $5.9\,\text{GHz}$. Fortunately, these two frequency bands are closely adjacent, leading to a balanced response. It is worth noting that our proposed metamaterial unit can support both the backward and forward propagations. Figure 10(b) depicts the normalized dispersion diagram which exhibits both negative and positive slopes for backward and forward wave propagations, respectively. These two types of propagation modes result in the emergence of two poles in the transmission responses of the proposed unit cells, called dual-mode responses. The attenuation constant curve, shown in Figure 10(b), is another parameter approving that the signals can pass through the proposed guide under the cutoff frequency, because the losses are very low. Moreover, a transition of the attenuation constant curve between the backward and forward propagation areas is smooth without any ripple.

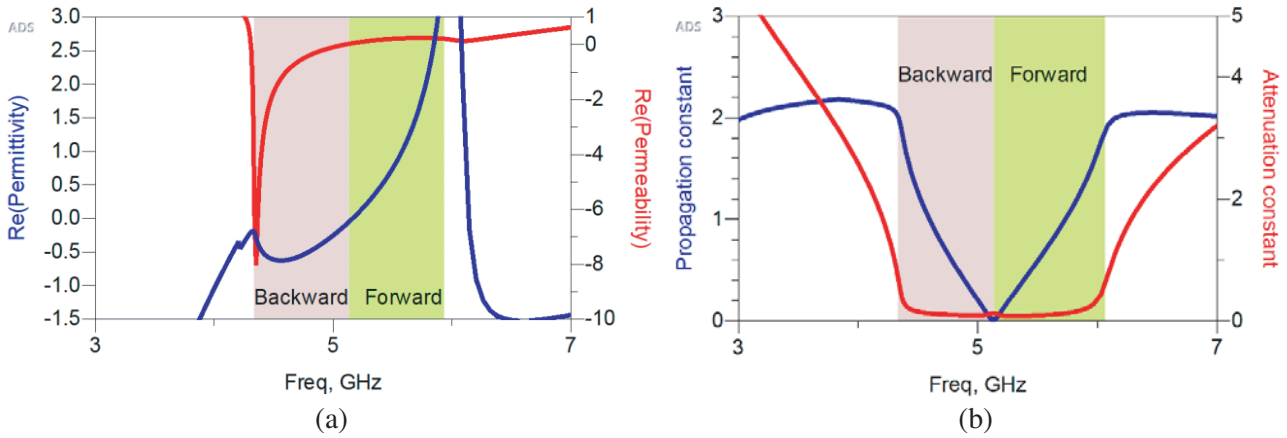

Figure 10. (a) Permittivity and permeability (constitutive parameters) of the 3rd iteration H-shaped fractal SIW-metamaterial unit cell, (b) propagation and attenuation constants of the 3rd iteration H-shaped fractal SIW-metamaterial unit cell.

2.4. Circuit Model and Losses

In this subsection, we establish the equivalent-circuit model which was used to predict the operation of the proposed unit cell, see Figure 11(a). The model starts by considering the SIW structure as a conventional two-wire transmission-line formed by the top wall of the SIW and the ground, connected to an infinite number of short-circuited stubs along the equivalent transmission-line. There are pieces of transmission-lines, connecting between an array of vias and the main two-wire transmission-line, so if we look from the center of the guide the short-circuited stubs appear as an equivalent inductance, represented by L_{via}. This inductance contributes to the highpass characteristics of the SIW structure. The equivalent transmission-line of the SIW can be represented as distributed shunt capacitance C_d and distributed series inductance L_d. The fractal slot is modeled by means of a series capacitance C_{frac}. The coupling between the fractal slot and the SIW is a combination of electric (capacitive) and magnetic types (inductive). Thus, C_c and L_c were used to describe these types of coupling. C_c indicates the capacitive connection between the ground of the SIW and small patches confined between the arms of the fractal slots. Because C_d is dominant, C_c is implicitly included within C_d. Thus, one can find

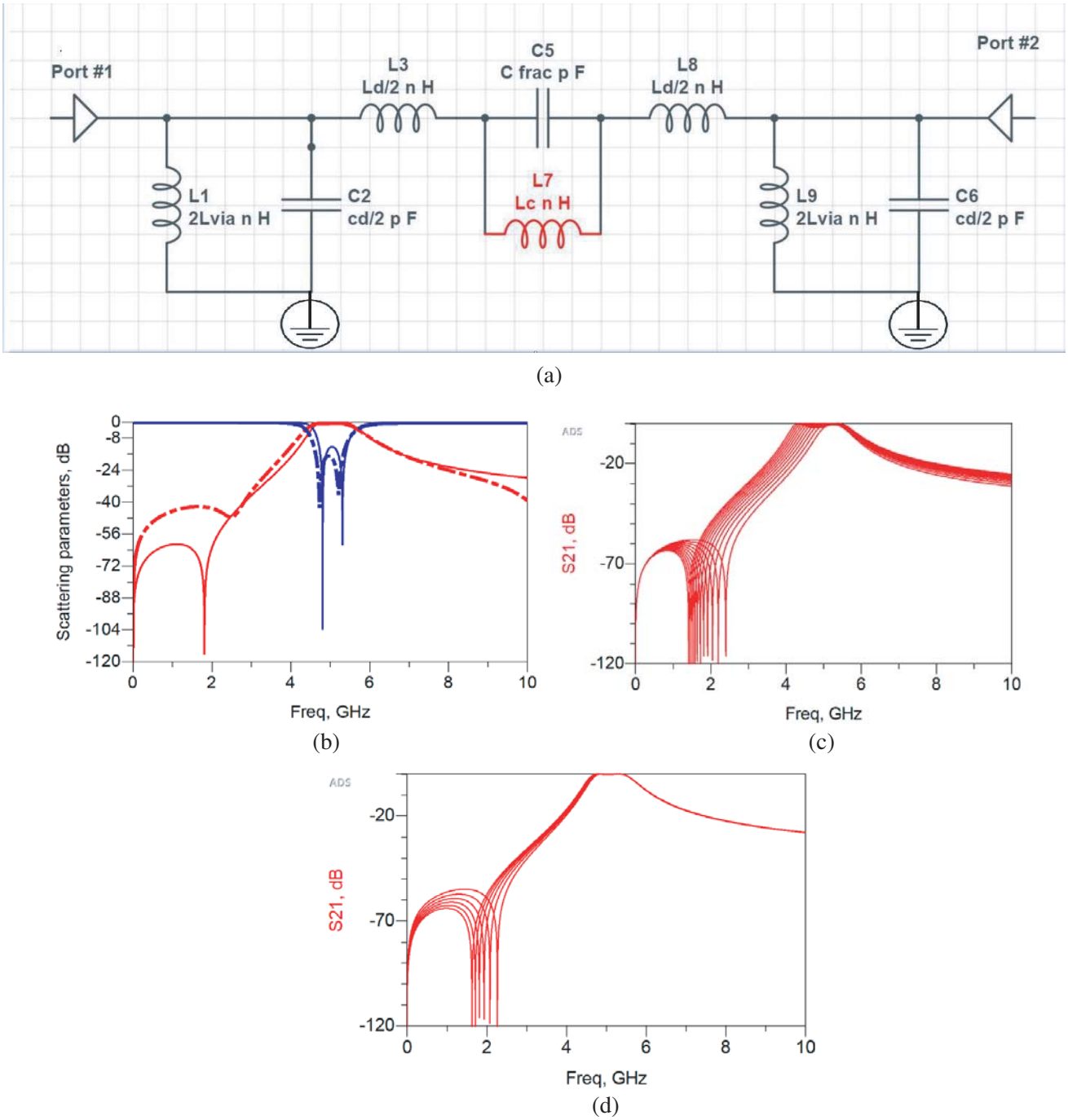

Figure 11. (a) The equivalent-circuit model of the H-shaped fractal SIW-metamaterial unit cell ($L_d = 1\,\text{pH}$, $L_c = 0.2\,\text{nH}$, $L_{via} = 8.3\,\text{nH}$, $C_d = 4.2\,\text{pF}$, and $C_{frac} = 0.93\,\text{pF}$), (b) a comparison between the frequency (scattering) response of the 3rd iteration H-shaped fractal SIW-metamaterial unit cell and its equivalent circuit model, (c) and (d) the frequency (scattering) response of the equivalent circuit model with varying C_{frac} and L_c, respectively.

C_d in our derived formulas but is not found in the equivalent circuit model. The inductive coupling, which is realized by the SIW structure and fractal slots, is given by L_c. The proposed circuit model is only valid for a limited range of frequencies, and the influence of high-order modes of resonators cannot be reflected by this equivalent-circuit model. Moreover, material, dielectric, and radiation losses are ignored for the sake of simplicity.

Although we consider a simple circuit model, it is clearly accurate and fully predicts the transmission characteristics of the proposed unit cells. Figure 11(b) compares between the results obtained from the full-wave simulation using the advanced design system ADS simulator and the circuit model. Values of the equivalent lumped elements are given in the caption of Figure 11. These lumped element values were obtained using the built-in optimization tool in ADS. Several hundreds of iterations were run to match between frequency responses of both the full-wave electromagnetic solver and the circuit model. However, there is a discrepancy because impacts of different factors have been ignored in the equivalent circuit model. We can infer from the circuit model impacts of equivalent lumped elements on the whole response of the unit cell, so we can configure the unit cell dimensions to realize any desired frequency response as explained in the following.

The frequency of the first transmission zero occurring below the passband is given by Eq. (2)

$$f_z = \frac{1}{2\pi\sqrt{L_c C_{frac}}} \tag{2}$$

L_c governs the location of the transmission zero. As L_c increases, the transmission zero is shifted down to lower frequencies. As known, when the locations of transmission zeros are closer to a passband, it exhibits a tremendously sharp rejection roll-off and leads to enhancing the filter selectivity. A strength of the magnetic coupling between the fractal slot and the SIW determines the value of L_c. In other words, a location of the fractal slot and slot width g govern the value of L_c. Thus, we can vary the location of the first transmission zero once we change a location of fractal slot which in turn varies L_c, see Figure 11(d). Moreover, all proposed unit cells are dual-mode structures. The dual-mode response is not clear in the response of the 1st iteration H-shaped fractal SIW-metamaterial unit cell because of the weak coupling between the slot and SIW. L_d and C_{frac} control the frequency of the 1st mode. In other words, the substrate's dielectric constant and thickness, size and width of the fractal slot are the main parameters which determine values of these two equivalent lumped elements. The frequency of the first mode is

$$f_{1st\text{-}mode} = \frac{1}{2\pi\sqrt{(L_d + L_{via})\,(C_{frac} + C_d + C_c)}} \tag{3}$$

As can be seen, C_{frac} contributes to both frequencies of the transmission zero and the 1st mode simultaneously. The frequency of the 2nd mode is

$$f_{2nd\text{-}mode} = \frac{1}{2\pi\sqrt{L_{via}\,(C_d + C_c)}} \tag{4}$$

This analysis aids to know which parameter can be used to evaluate the response of the proposed unit cells. However, some of these parameters cannot be altered after selecting the dimensions of the initial SIW such as C_d, L_d, and L_{via}. However, C_c and C_{frac} are the most important parts which play a vital role in determining the frequency of the proposed unit cells. Figures 11(c) and (d) show the responses of the equivalent-circuit model when varying C_{frac} and L_c, respectively. As C_{frac} increases, both the transmission zero and the 1st mode tend to reach a lower frequency, whereas only the transmission zero varies with the varying value of L_c. From the circuit analysis, we can establish a procedure connecting between the circuit model and the electromagnetic unit cell structures but is left as a future work.

Next, as the slots are etched on the top walls of the SIW structures and are not fully covered, radiation losses are expected. Losses in our proposed unit cells are considered as a practical issue confronted during the design. However, according to calculations, we found that the radiations losses were not significant, being less than 0.03 in a whole band. If we consider other losses such as dielectric and conductor losses in our calculations, the total losses become less than 0.176, see Figure 12. These losses were normalized and calculated using the formula in Eq. (5).

$$Losses = 1 - |S_{21}|^2 - |S_{11}|^2 \tag{5}$$

Radiation losses increased as the slot width increased, leading to an increase in power leaked to space. Since the fractal slot acts as a magnetic diploe, it works similarly to a magnetic dipole antenna. The very small radiation will be normal on the structure, and it can be easily avoided by shielding the structure. The adjacent components will not be largely affected. Compared to [5, 30], the radiation losses in the proposed unit cells are smaller. In addition to the property of low radiation loss, they offer advantages in terms of size and selectivity.

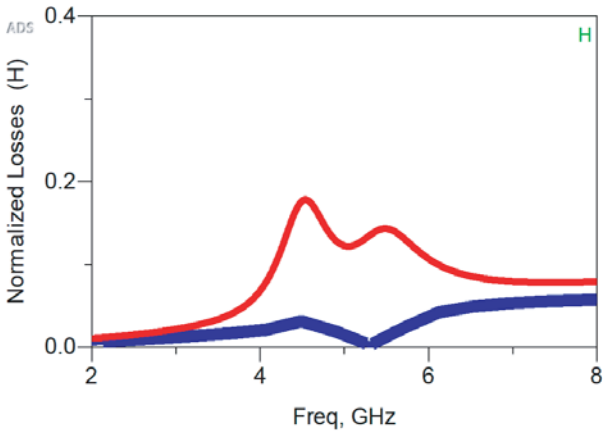

Figure 12. Calculated total losses (red line) and only radiation losses (blue line) for the 3rd iteration H-shaped fractal SIW-metamaterial unit cell.

3. FILTER DESIGN METHODOLOGY

Having investigated and discussed the proposed metamaterial unit cells (resonators) earlier in this paper, now we will follow the regular procedure (classical methodology) to synthesize filters using only the proposed 3rd iteration H-shaped fractal SIW-metamaterial unit cell [31]. The regular method used to meet the given design specifications depends on the coupling coefficient k and the external quality factor Q_{ext}. Three different filters were simulated using the advanced design system ADS simulator based on the momentum. The 3rd iteration H-shaped fractal SIW-metamaterial unit cell shown in Figure 6(d) is the basis of these three filters which are the one, three, and five stages SIW-metamaterial filters, presented in this section. In other words, number of the filter stage is according to how many unit cells are used in the proposed filters, see Figure 13. Although the proposed SIW-metamaterial unit cells offer transmissions of passbands under the cutoff frequency of the initial SIW structures, there is no control on their bandwidths and scattering parameters S. Fortunately, the interaction between the fractal slots and SIW structures can increase the degree of freedom to properly obtain the required filter specifications. The filter design method will be briefly deliberated in this section exploiting the conventional coupled resonators scheme. The design process is outlined in the beginning, and then a simple illustration is provided to give some useful guidelines. In the first step, the circuit synthesis based on filter requirements is introduced. The external quality factor and coupling coefficient parameters being the basis of the filter design can be determined in terms of the low-pass filter circuit elements. Calculating these two parameters aids to establish a relationship between the SIW-fractal slot interaction which in turn determines the physical dimensions of the filters and the low-pass filter circuit elements.

In general, all the proposed unit cells have dual poles (i.e., dual modes) in their responses as mentioned above. These two separate resonance frequencies are useful to extract the coupling coefficient and external quality factor. The coupling coefficient is given by:

$$k = \frac{f_2^2 - f_1^2}{f_2^2 + f_1^2} \tag{6}$$

and the external quality factor is given by:

$$Q_{ext} = \frac{2f_o}{BW} \tag{7}$$

where f_2 and f_1 refer to frequencies of the higher and lower modes of the electromagnetically coupled fractal slot resonator with the SIW structure. f_o stands for the central resonance frequency, and BW is the 3 dB bandwidth.

Some design dimensions were carefully tuned during investigations to extract both the coupling coefficient k and the external quality factor Q_{ext}. Thus, we can establish two curves for the coupling

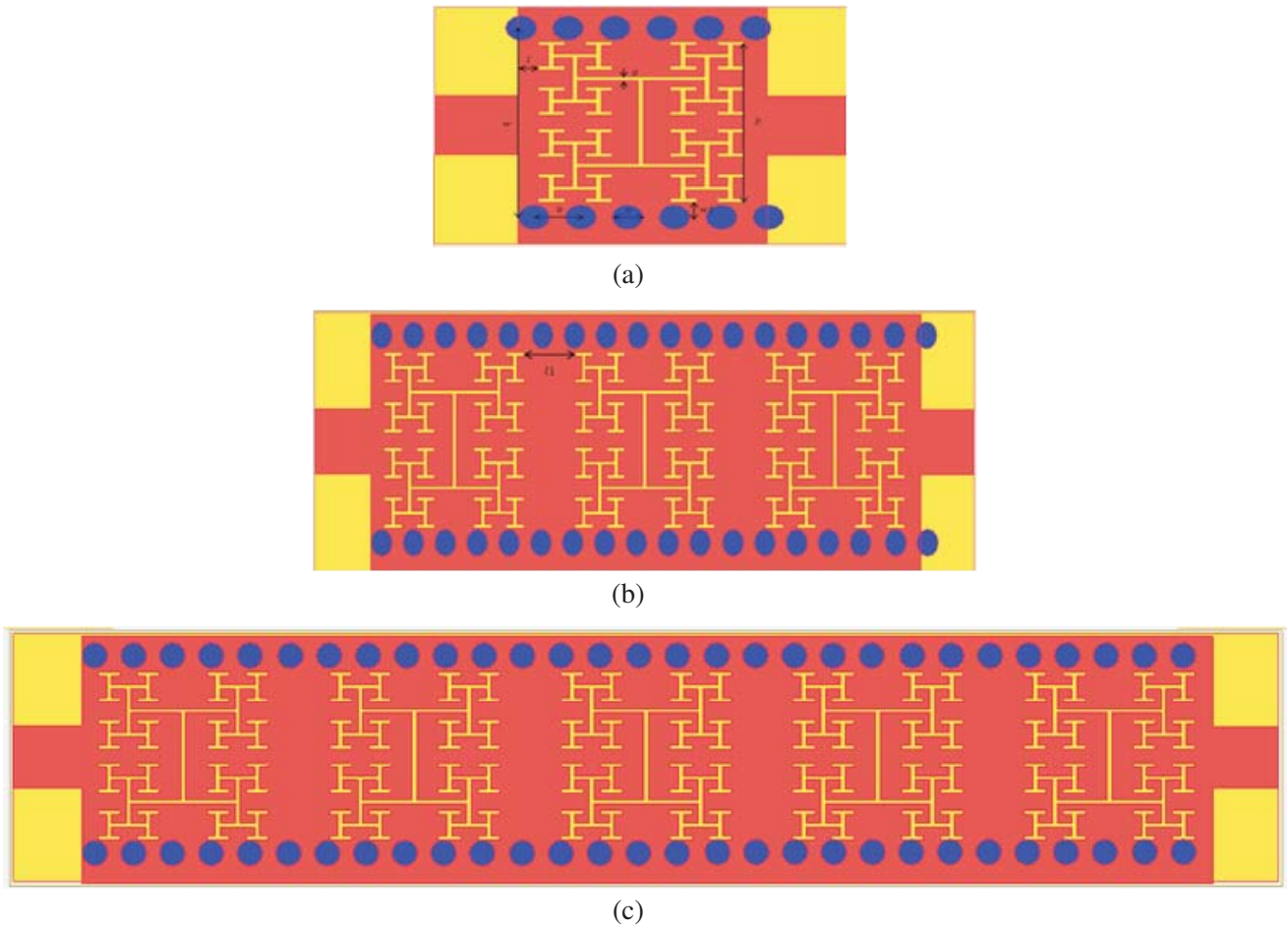

(a)

(b)

(c)

Figure 13. Configurations of (a) one stage 3rd iteration H-shaped fractal SIW-metamaterial bandpass filter, (b) three stages 3rd iteration H-shaped fractal SIW-metamaterial bandpass filter, (c) five stages 3rd iteration H-shaped fractal SIW-metamaterial bandpass filter ($w = 7.8\,\text{mm}$, $w_1 = 0.68\,\text{mm}$, $l = 0.8\,\text{mm}$, $l_1 = 2.39\,\text{mm}$, $a = 1\,\text{mm}$, $b = 1.5\,\text{mm}$, $p = 6.4\,\text{mm}$, $g = 0.15\,\text{mm}$).

coefficient and the external quality factor versus physical dimensions of the proposed filters in an effort to facilitate optimizing the design. For the sake of simplicity, parameters k and Q_{ext} are only shown for the proposed one stage 3rd iteration H-shaped SIW-metamaterial filter. After determining k and Q_{ext}, the optimized physical dimensions of the three filters presented in this paper can be established.

For illustration, a simple example is given. In this example, a one stage SIW-metamaterial filter utilizing single 3rd iteration H-shaped fractal slot is placed in the middle of the guide, see Figure 13(a). The physical dimensions w_1 and l of the filter shown in the figure are changed to calculate parameters k and Q_{ext} following the procedure explained above. The filter has a passband located about 5.3 GHz with about a 0.65 GHz bandwidth. Although the SIW is incorporated with a single fractal slot, its response is dual modes. Thus, a second order circuit synthesis is carried out where $k_{12} = k_{21} = 0.052$ and $Q_{ext} = 25.3$. The electromagnetic simulation is used to determine the initial dimensions of the resonator (i.e., unit cell). The external quality factor is preferred to be higher to see clearly the two resonance frequencies of the dual mode behavior, known as even and odd as well.

In Figure 14(a), the external quality factor and the coupling coefficient of the one stage 3rd iteration H-shaped SIW-metamaterial filter versus the physical dimensions w_1 have been plotted, while Figure 14(b) shows these two parameters versus l for the same filter. These two plots expedite the procedure to obtain the proper dimensions to design a filter with required properties. Figures 14(c) and 14(d) exhibit current distributions of the low and high modes, respectively.

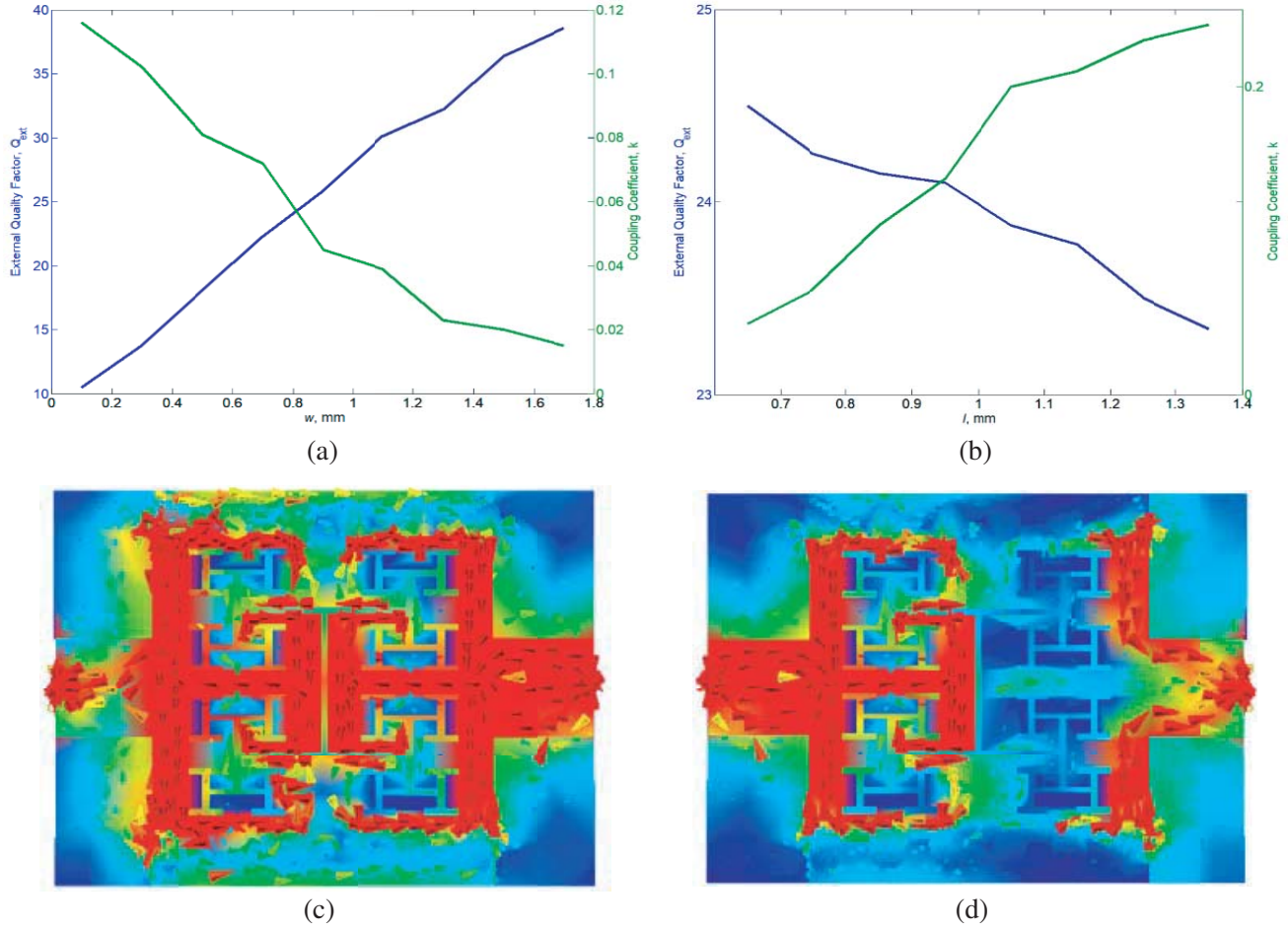

Figure 14. Coupling coefficients and external quality factors for the one stage 3rd iteration H-shaped fractal SIW-metamaterial filter as a function of (a) w_1, (b) l, (c) current distribution for low mode, (d) current distribution for high mode.

These initial dimensions dependent on the design curves were optimized using the electromagnetic ADS simulator. Also, there are other physical dimensions considered in filter designs, but they are not provided here. The remaining two filters presented in this paper have been optimized following the same procedure used in the previous filter.

As illustrated, the coupling coefficient and the external quality factor can be controlled in several ways. Meanwhile, we can use the equivalent circuit model demonstrated above to assist in determining some design properties such as governing the transmission zeroes and bandwidths. The space between the vias and the fractal slot w_1 as well as the space between feeding edge and the fractal slot l play a vital role in determining the filter bandwidth as can be seen in Figure 14. Increasing w_1 leads to decreasing k and increasing Q_{ext} while increasing l leads to increasing k and decreasing Q_{ext}. In the first case, the cutoff frequency becomes lower, and the current distribution of the fundamental mode occupies bigger area. Therefore, the coupling between the fractal slot and SIW becomes less. In contrast, the cutoff frequency remains the same in the second case, but the slot interacts effectively with SIW guide, leading to obtaining higher coupling. Varying l does not change k and Q_{ext} as much as w_1 does for the same reasons mentioned above.

However, obtaining proper physical dimensions is critical because of the overall size. Thus, compromise between the performance and the design requirements from one side and the size from another side is necessary. The final filter configuration is chosen according to w_1 and l with 0.8 mm and 0.65 mm, respectively. Figure 13 also shows the design layouts of the three and five stages SIW-

metamaterial filters. Physical dimensions of these two filters have been determined after a huge amount of tuning and optimization using the electromagnetic solver. It is important to bear in mind that the increase in number of usage slots represents the increase in the filter order.

4. SIMULATION AND MEASUREMENT RESULTS

This section is devoted to demonstrating and practically validating the proposed filters developed in the previous sections. Photographs of the fabricated filters are shown in Figure 15. The filter stage relies on a number of fractal slots etched in each SIW structure as illustrated in Figures 13 and 15. The 3rd iteration H-shaped fractal slots are etched over the top walls of the SIW structures, and they are placed linearly along the printed guide (SIW). An FR4 substrate having a thickness of 1.2 mm and a relative permittivity 4.6 was used in all fabrications using the standard printed circuit board (PCB) process in the Electrical Engineering Department, University of Tun Hussein Onn Malaysia UTHM in Malaysia. Dielectric and metallic losses were considered in all simulations by using the tangent loss ($\tan d$) of 0.01 for substrate and the conductivity (σ) of $5.8 \times 10e^7$ S/m for copper, respectively. The vector network analyzer VNA was used to measure and evaluate filters' performances. The measured data were compared with the simulated one, and the agreement between them was very good.

Figure 15. A photograph of the fabricated SIW-metamaterial filters.

The fabricated filters shown in Figure 15 are very compact although they fall within a category of waveguide filters. Physical dimensions of the filters are all given within the caption of Figure 13. The three filters were designed following the formerly mentioned procedure given in the previous section. Figure 16 compares between the measured (solid line) and simulated (dashed line) frequency responses of the one stage 3rd iteration H-shaped fractal SIW-metamaterial filter. As expected, this filter has transmission characteristics similar to what the 3rd iteration H-shaped fractal SIW-metamaterial unit cell has because both of them consist of single unit cells. The 3 dB bandwidth was about 0.65 GHz and the center frequency about 5.3 GHz with two poles in the passband. Thus, the fractional bandwidth was approximately 122%, achieving a broadband filter because of its high internal coupling coefficient and low external quality factor. Furthermore, the slots can be scaled up or down to obtain any frequency of interest. Furthermore, two zeros can be observed, located around 4.4 GHz and 7.2 GHz, respectively. Its maximum simulated transmission coefficient (i.e., insertion loss) was 0.5 dB while the measured insertion loss was approximately 1.5 dB, which includes losses caused by the SMA connectors not considered in the simulation. The minimum in-band reflection coefficient (i.e., return loss) of the simulated result was

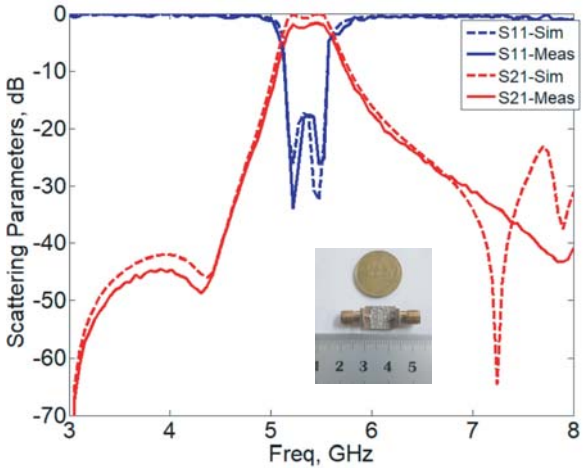

Figure 16. Measured (solid line) and simulated (dashed line) transmission response of the one stage 3rd iteration H-shaped fractal SIW-metamaterial bandpass filter (S_{11} is red and S_{21} is blue curves.).

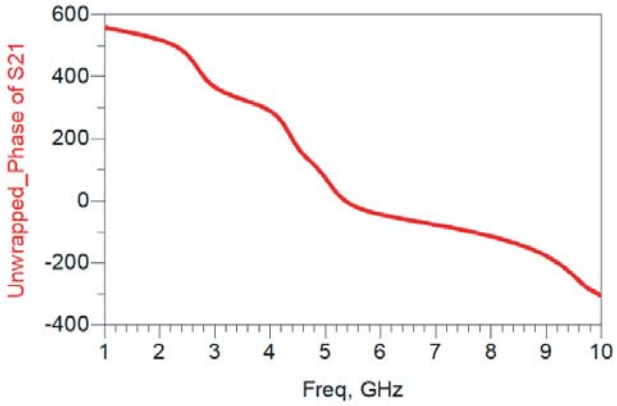

Figure 17. Measured unwrapped phase of S_{21} response of the one stage 3rd iteration H-shaped fractal SIW-metamaterial filter.

about 19 dB which is almost the same as the measured one. As known, the presence of transmission zeros in frequency responses aids to increase the filter selectivity. As illustrated in the results, the measured rejection in the lower stopband was about 45 dB, while it is equal to 30 dB in upper stropband. Figure 17 shows the measured unwrapped phase response of the proposed one stage filter. As can be seen, the phase is positive (phase-lead) and decreased to become negative (phase-lag) in the passband from about 5.05 GHz to 5.7 GHz. Varying the phase from the positive to negative confirms that there are two natures for the wave propagation within the passband, the backward and forward wave propagations.

It is worth noting that this filter is very compact where its overall physical size is $7.5 \times 8\,\text{mm}^2$ or $0.12\lambda_g \times 0.15\lambda_g$, where λ_g is the guided wavelength at a center frequency of 5.3 GHz.

The simulated (dashed line) and measured (solid line) frequency responses of the three and five stages 3rd iteration H-shaped fractal SIW-metamaterial filters are portrayed in Figures 18(a) and (b), respectively. Six poles are clearly observed in Figure 18(a), while there are eight poles for the filter presented in Figure 18(b). The second filter has two zeros placed before and after the passband, and the third filter has three transmission zeros. As the number of transmission zeros increases, the filter response roll-off becomes very sharp. For the second filter, the measured 3 dB bandwidth and center frequency are about 1.2 GHz and 5 GHz, respectively, while the measured 3 dB bandwidth is 1.3 GHz, and the center frequency is 5 GHz for the third filter. As can be seen, the center frequency of the proposed one stage filter is shifted down to become around 5 GHz for the proposed three and five stages

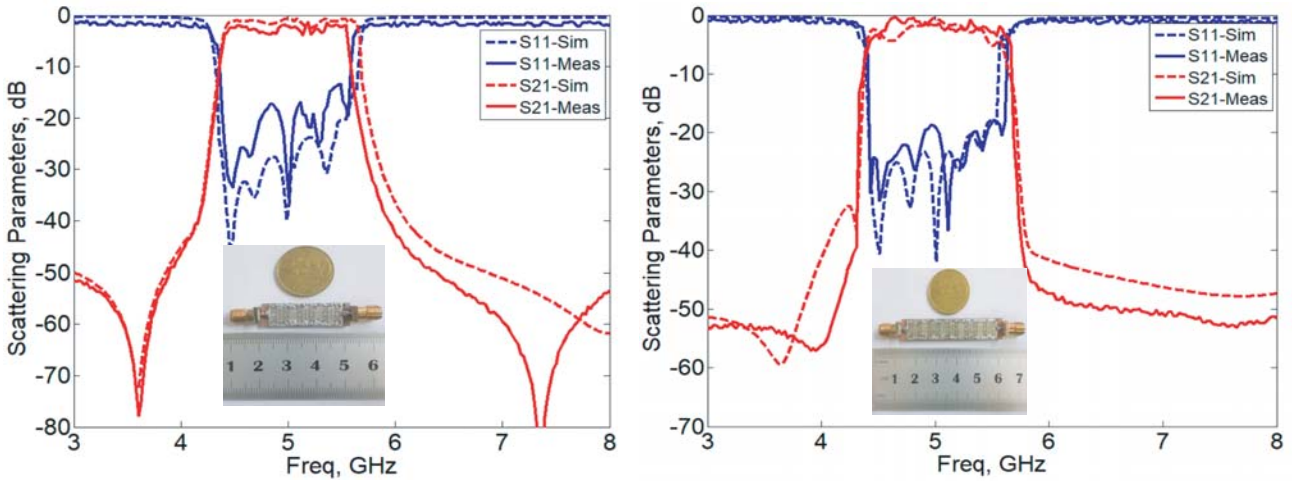

Figure 18. Measured (solid line) and simulated (dashed line) transmission response of (a) the three stage 3rd iteration H-shaped fractal SIW-metamaterial filter, (b) the five stage 3rd iteration H-shaped fractal SIW-metamaterial filter (S_{11} is red and S_{21} is blue curves.).

filters. This is normal because of electromagnetic coupling between slots for filters with more slots. Also, the bandwidth becomes wider for the last two filters.

Table 1 summarizes the measured maximum in-band insertion loss and measured minimum in-band return loss for the second and third filters. The stopband rejection was highly improved as a filter order increased and quickly went below 45 dB up to 8 GHz for the second filter. It was about 50 dB up to 8 GHz for the third filter. As anticipated, the measured results agree very well with the simulated

Table 1. A summary of the measured in-band return and insertion losses.

Filter Stage No.	Maximum in-band Insertion Loss (measured)	Minimum in-band Return Loss (measured)
Three	2.5 dB	14 dB
Five	1.8 dB	17 dB

Table 2. A comparison of the proposed one stage filter with other works.

Reference	Fractional Bandwidth (%)	Insertion Loss (dB)	Return Loss (dB)	Size ($\lambda_g \times \lambda_g$)
[32]	5.2	4	12	0.3663×0.24
[5]	11.2	1.6	15	0.263×0.146
[33]	7	1.9	20	0.333×0.65
[34]	9.6	1.22	15	0.463×0.22
[35]	11	1.2	16.7	0.2053×0.166
[36]	10.9	1.2	35	0.183×0.09
[37]	8.3	1.2	20	0.075×0.075
[38]	8.2	0.5	10	0.34×0.15
This work	12.25	0.75	23	0.12×0.15

ones. However, slight discrepancies between the measured and simulated results are by many reasons such as using ideal environments in simulations, errors in fabrications, and losses in measurements. Therefore, our proposed designs tend to increase the out-of-band rejection as number of slots used in designs increases at the cost of size.

Table 2 introduces the comparison of the proposed one stage 3rd iteration H-shaped SIW-metamaterial filter with other reported SIW based metamaterial bandpass filters. Compact size, high rejection, easy integration, frequency scale, and small insertion loss are the advantages that our proposed filters have.

5. CONCLUSION

In this study, new SIW-metamaterial unit cells were designed and investigated. Instead of using CSRR inclusions as in the conventional SIW-metamaterial unit cells, fractal slots were etched over the top walls of the SIW structures. The 3rd iteration of the H-shaped fractal curve was selected to get more compact unit cells compared to other fractal iterations. Both backward and forward wave propagations were supported under the cutoff frequency of the SIW with two passbands being closely adjacent. The permittivity, permeability, and dispersion diagram were extracted using the s-parameters to approve the metamaterial concepts. Furthermore, the equivalent circuit model of the proposed unit cell was established and analyzed.

Afterwards, different filters with different stages which were one, three, and five stages were designed, simulated, fabricated, and tested. Based on these passbands, a different family of bandpass filters supporting both backward and forward wave propagations were presented for the first time according to the best of authors' knowledge. Both the external quality factors and coupling coefficients, which are important parameters in the classical filter design methodology, versus some physical dimensions, were explored to obtain the required properties of filters. The proposed SIW-metamaterial unit cells and filters offer several advantages such as compact sizes, easy integration with other PCB components and capability to scale-up or down, broadband frequency responses, high selectivity with the aid of existence of the transmission zeros, low insertion loss, and low cost. Measured and simulated results were in good agreement. Thus, these significant advantages enable our new filters based on fractal slots to be suitable for practical applications.

REFERENCES

1. Deslandes, D. and K. Wu, "Integrated microstrip and rectangular waveguide in planar form," *IEEE Microw. Wirel. Components Lett.*, Vol. 11, No. 2, 68–70, 2001.
2. Cassivi, Y., L. Perregrini, P. Arcioni, M. Bressan, K. Wu, and G. Conciauro, "Dispersion characteristics of substrate integrated rectangular waveguide," *IEEE Microw. Wirel. Components Lett.*, Vol. 12, No. 9, 333–335, 2002.
3. Deslandes, D. and K. Wu, "Design consideration and performance analysis of substrate integrated waveguide components," *2002 32nd Eur. Microw. Conf. EuMC 2002*, No. 2, 3–6, 2002.
4. Musallam, M., et al., "Metabolic Syndrome and its components among Qatari population," *Int. J. Food Safety, Nutr. Public Heal.*, Vol. 1, No. 1, 88–102, 2008.
5. Dong, Y. D., T. Yang, and T. Itoh, "Substrate integrated waveguide loaded by complementary split-ring resonators and its applications to miniaturized waveguide filters," *IEEE Trans. Microw. Theory Tech.*, Vol. 57, No. 1, 2211–2223, 2009.
6. Veselago, V. G., "The electrodynamic of substances with simultaneous negative values of ε and μ," *Sov. Phys. Uspekhi*, Vol. 10, No. 4, 509–514, 1968.
7. Gil, I., J. Bonache, J. García-García, F. Falcone, and F. Martín, "Metamaterials in microstrip technology for filter applications," *IEEE Antennas Propag. Soc. AP-S Int. Symp.*, Vol. 1A, No. 1, 668–671, 2005.
8. Navarro-Cia, M., M. Beruete, I. Campillo, and M. Sorolla, "Millimeter-wave left-handed extraordinary transmission metamaterial demultiplexer," *IEEE Antennas Wirel. Propag. Lett.*, Vol. 8, 212–215, 2009.

9. Shelby, R. A., D. R. Smith, and S. Schultz, "Experimental verification of a negative index of refraction," *Science*, Vol. 292, No. 5514, 77–79, 2001.
10. Falcone, F., T. Lopetegi, J. D. Baena, R. Marqués, F. Martín, and M. Sorolla, "Effective negative-ε stopband microstrip lines based on complementary split ring resonators," *IEEE Microw. Wirel. Components Lett.*, Vol. 14, No. 6, 280–282, 2004.
11. Marqus, R., F. Martn, and M. Sorolla, *Metamaterials with Negative Parameters*, 2007.
12. Caloz, C., *Electromagnetic Metamaterials Transmission Line Theory and Microwave Applications: The Engineering Approach*, 2005.
13. Martinez, J. A., J. J. De Dios, A. Belenguer, H. Esteban, and V. E. Boria, "Integration of a very high quality factor filter in empty substrate-integrated waveguide at Q-band," *IEEE Microw. Wirel. Components Lett.*, Vol. 28, No. 6, 503–505, 2018.
14. Moro, R., S. Moscato, M. Bozzi, and L. Perregrini, "Substrate integrated folded waveguide filter with out-of-band rejection controlled by resonant-mode suppression," *IEEE Microw. Wirel. Components Lett.*, Vol. 25, No. 4, 214–216, 2015.
15. Kumar, R. and S. N. Singh, "Design and analysis of ridge substrate integrated waveguide bandpass filter with octagonal complementary split ring resonator for suppression of higher order harmonics," *Progress In Electromagnetics Research C*, Vol. 89, 87–99, 2019.
16. Hong, W., et al., "Half mode substrate integrated waveguide: A new guided wave structure for microwave and millimeter wave application," *IRMMW-THz 2006 — 31st Int. Conf. Infrared Millim. Waves 14th Int. Conf. Terahertz Electron.*, Vol. 152, 219, 2006.
17. Structures, W. L., Y. Dong, S. Member, T. Itoh, and L. Fellow, "Composite right/left-handed substrate integrated waveguide and half mode substrate integrated," Vol. 59, No. 3, 767–775, 2011.
18. Huang, X. L., L. Zhou, M. Völkel, A. Hagelauer, J. F. Mao, and R. Weigel, "Design of a novel quarter-mode substrate-integrated waveguide filter with multiple transmission zeros and higher mode suppressions," *IEEE Trans. Microw. Theory Tech.*, Vol. 66, No. 12, 5573–5584, 2018.
19. Dong, Y. D. and T. Itoh, "Composite right/left-handed substrate integrated waveguide and half-mode substrate integrated waveguide," *IEEE MTT-S Int. Microw. Symp. Dig.*, 49–52, 2009.
20. Zhang, X. C., Z. Y. Yu, and J. Xu, "Novel band-pass Substrate Integrated Waveguide (SIW) filter based on Complementary Split ring Resonators (CSRRs)," *Progress In Electromagnetics Research*, Vol. 72, 39–46, 2007.
21. Che, W., C. Li, K. Deng, and L. Yang, "A novel bandpass filter based on complementary split rings resonators and substrate integrated waveguide," *Microw. Opt. Technol. Lett.*, Vol. 50, No. 3, 748–753, 2008.
22. Cao, H., et al., "A CSRR-fed SIW cavity-backed fractal patch antenna for wireless energy harvesting and communication," *Sensors (Switzerland)*, Vol. 15, No. 9, 21196–21203, 2015.
23. Danaeian, M., K. Afrooz, and A. Hakimi, "Miniaturization of substrate integrated waveguide filters using novel compact metamaterial unit-cells based on SIR technique," *AEU — Int. J. Electron. Commun.*, Vol. 84, 62–73, 2018.
24. Dong, Y. and T. Itoh, "Miniaturized substrate integrated waveguide slot antennas based on negative order resonance," *IEEE Trans. Antennas Propag.*, Vol. 58, No. 12, 3856–3864, 2010.
25. Peano, G., "Sur une courbe, qui remplit toute une aire plane," *Math. Ann.*, Vol. 36, No. 1, 157–160, 1890.
26. Bao, X. L., G. Ruvio, M. J. Ammann, and M. John, "A novel GPS patch antenna on a fractal hi-impedance surface substrate," *IEEE Antennas Wirel. Propag. Lett.*, Vol. 5, No. 1, 323–326, 2006.
27. Romeu, J. and Y. Rahmat-Samii, "Fractal FSS: A novel dual-band frequency selective surface," *IEEE Trans. Antennas Propag.*, Vol. 48, No. 7, 1097–1105, 2000.
28. Murad, N. A., M. Esa, M. F. Mohd Yusoff, and S. H. Ammah Ali, "Hilbert curve fractal antenna for RFID application," *2006 Int. RF Microw. Conf. Proc.*, Vol. 00, 182–186, 2006.
29. Palandoken, M. and H. Henke, "Fractal negative-epsilon metamaterial," *Final Progr. B. Abstr. — iWAT 2010 2010 Int. Work. Antenna Technol. Small Antennas, Innov. Struct. Mater.*, No. 1, 2–5, 2010.

30. J. García-García, J. Bonache, I. Gil, F. Martín, M. Del Castillo Velázquez-Ahumada, and J. Martel, "Miniaturized microstrip and CPW filters using coupled metamaterial resonators," *IEEE Trans. Microw. Theory Tech.*, Vol. 54, No. 6, 2628–2634, 2006.
31. Hong, J.-S. and M. J. Lancaster, *Microstrip Filters for RF/Microwave Applications*, Vol. 7, 2001.
32. Huang, L., I. D. Robertson, W. Wu, and N. Yuan, "Substrate integrated waveguide filters with broadside-coupled complementary split ring resonators," *IET Microwaves, Antennas Propag.*, Vol. 7, No. 10, 795–801, 2013.
33. Yan, T., X.-H. Tang, and Z.-X. Xu, "A novel type of bandpass filter using complementary open-ring resonator loaded HMSIW with an electric cross-coupling," *Microw. Opt. Technol. Lett.*, Vol. 58, No. 4, 748–753, 2016.
34. Silveira, D., et al., "Improvements and analysis of nonlinear parallel behavioral models," *Int. J. RF Microw. Comput. Eng.*, Vol. 19, No. 5, 615–626, 2009.
35. Wu, L. S., X. L. Zhou, W. Y. Yin, L. Zhou, and J. F. Mao, "A substrate-integrated evanescent-mode waveguide filter with nonresonating node in low-temperature co-fired ceramic," *IEEE Trans. Microw. Theory Tech.*, Vol. 58, No. 10, 2654–2662, 2010.
36. Danaeian, M., K. Afrooz, A. Hakimi, and A. R. Moznebi, "Compact bandpass filter based on SIW loaded by open complementary split-ring resonators," *Int. J. RF Microw. Comput. Eng.*, Vol. 26, No. 8, 674–682, 2016.
37. Danaeian, M., A. R. Moznebi, and K. Afrooz, "A novel super compact half-mode substrate-integrated waveguide filter using modified complementary split-ring resonator," *Int. J. RF Microw. Comput. Eng.*, Vol. 29, No. 6, 1–8, 2019.
38. Azad, A. R. and A. Mohan, "Sixteenth-mode substrate integrated waveguide bandpass filter loaded with complementary split-ring resonator," *Microw. Opt. Technol. Lett.*, Vol. 53, No. 8, 546–547, 2017.